

Partial-Range SOC-Insensitive Model With EIS Change Pattern Recognition Model for Battery Aging Estimation

Zhansheng Ning , Student Member, IEEE, Junyun Deng ,
Prasanth Venugopal , Senior Member, IEEE, Thiago Batista Soeiro , Senior Member, IEEE,
and Gert Rietveld , Senior Member, IEEE

Abstract—Electrochemical impedance spectroscopy (EIS) holds significant potential for evaluating battery degradation. However, EIS readings are not only affected by battery degradation but also by the state of charge (SOC). Traditional models for estimating battery capacity rely on impedances measured at specific SOC points, and thus can suffer from substantial inaccuracies when SOC estimation errors occur. To tackle this challenge, we propose a novel partial-range SOC-insensitive model for precise battery capacity estimation using transformer neural networks complemented by an EIS change pattern model based on the k-nearest neighbors (KNN) algorithm. To the best of our knowledge, this is the first study to develop an EIS-based battery capacity model that considers incorrect SOC scenarios. Test results show that our partial-range SOC-insensitive model can estimate battery capacity with a root-mean-square percentage error of 2.69%, even with a 30% SOC error, within the SOC range of 20% to 50%. Adding the EIS change pattern recognition model further improves the performance of the partial-range SOC-insensitive model, reducing the maximum absolute percentage error from 19% to less than 3% in scenarios involving 50% to 70% SOC error during battery cell testing.

Index Terms—Capacity estimation, electrochemical impedance spectroscopy (EIS) change pattern recognition, k-nearest neighbor (KNN), li-ion battery, state of charge (SOC)-insensitive, transformer.

Received 28 May 2024; revised 3 September 2024 and 18 October 2024; accepted 21 November 2024. This work was supported in part by the project SEANERGETIC with Project KICH1.KICH1.21.003 of the Research Program Zero Emission and Circular Shipping (KIC) which is financed by the Dutch Research Council (NWO). (Corresponding author: Zhansheng Ning.)

Zhansheng Ning, Junyun Deng, Prasanth Venugopal, and Thiago Batista Soeiro are with the Faculty of Electrical Engineering, Mathematics and Computer Science (EEMCS), University of Twente, 7522 NB Enschede, The Netherlands (e-mail: z.ning@utwente.nl; j.deng@utwente.nl; prasanth.venugopal@utwente.nl; t.batistasoeiro@utwente.nl).

Gert Rietveld is with the Faculty of Electrical Engineering, Mathematics and Computer Science (EEMCS), University of Twente, 7522 NB Enschede, The Netherlands, and also with VSL, 2629 JA Delft, The Netherlands (e-mail: gert.rietveld@vsl.nl).

Digital Object Identifier 10.1109/TIE.2024.3511086

I. INTRODUCTION

LITHIUM-ION batteries play an important role in the electrification of transportation. To guarantee the safety of the battery cell, battery management systems (BMS) are used with various functions, such as state of health (SOH) estimation [1], state of charge (SOC) and state of power (SOP) estimation [2], [3], and remaining useful life (RUL) prediction [4]. However, the efficacy of all these fundamental functions of the BMS hinges on precise battery capacity estimation. Hence, it is imperative to adopt advanced detection devices to acquire data reflecting the battery's internal state.

Next to conventional data derived from voltage, current, and temperature sensors, onboard electrochemical impedance spectroscopy (EIS) devices are regarded as a technology holding significant promise for enhancing battery degradation estimation. EIS captures impedance across a broad frequency spectrum and is recognized for its ability to provide comprehensive insights into material properties, interfacial phenomena, and electrochemical reactions [5] corresponding to battery degradation. Onboard EIS can be realized in several ways, such as through power converters such as the dc-dc converter in onboard chargers [6], the inverter within motor drivers [7], through dedicated smart integrated circuits [8], or by predicting EIS from pulse tests [9]. Whilst these methods are not yet fully applicable to vehicles, offline EIS remains a valuable reference and foundation for ongoing research.

Data-driven methods hold promise for battery capacity and aging estimation as they enable nonlinear mapping between measurement data and battery capacity without relying on an accurate physical or equivalent circuit model (ECM). Various methods can be used for this task: Gaussian process regression (GPR) and support vector machines (SVM) are easy to implement but struggle with large datasets [10], [11]. Convolutional neural networks (CNN) can automatically extract features and estimate battery capacity but are less suited for capacity prediction [12]. Long short-term memory (LSTM) networks can perform both battery capacity estimation and prediction, but they suffer from limitations such as long-term dependency issues and lack of parallel training [13]. In contrast, transformers are very promising for battery capacity estimation and prediction, as they address long-term dependency challenges and improve

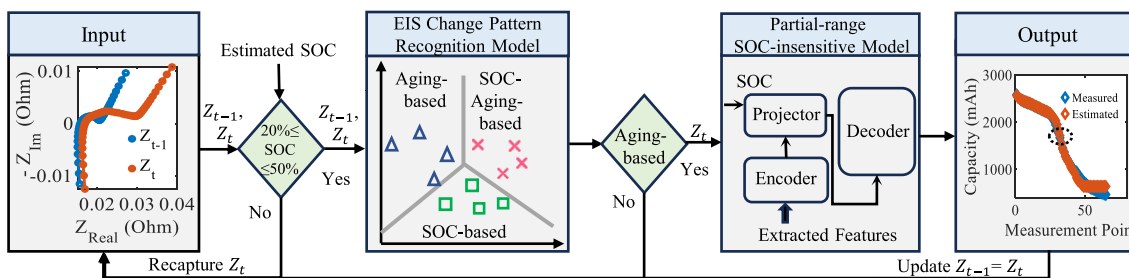


Fig. 1. Architecture of the proposed method. First, if the estimated SOC falls within the 20% to 50% range during the current cycle, Z_t is obtained and used as input for the EIS change pattern model. Otherwise, continue real-time monitoring of the estimated SOC in subsequent cycles until it falls within the 20% to 50% range, after which the EIS spectrum is measured and considered as Z_t . Second, if the change in Z_t is caused by the battery aging compared with Z_{t-1} , then Z_t is used as input for the partial-range SOC-insensitive model. Otherwise, the change in Z_t is influenced by an incorrect estimated SOC when compared with Z_{t-1} , and Z_t cannot be used as input for partial-range SOC-insensitive model. The model should then wait until the change in Z_t is caused solely by battery aging, relative to Z_{t-1} . Finally, obtain the estimated battery capacity.

training speed via their multihead attention architecture. The input to data-driven methods for battery capacity estimation consists of features that are highly related to battery aging [14]. This can be EIS features such as fixed frequency impedance, which utilizes impedance at specific frequencies such as 2.16 and 17.80 Hz [10] or broadband frequency, which employs impedance ranging from 0.02 to 20 kHz [15]. An alternative is the ECM approach, where EIS-based parameters from the fractional-order ECM serve as features [16].

The aforementioned features serve as inputs to machine learning models for battery capacity estimation. However, most of these features are extracted, and models are trained at a single SOC. For example, GPR models have been developed based on impedance measured at 0% SOC, and 100% SOC, respectively [17]. In [18], two generative adversarial network (GAN) models are developed based on impedance measured at 33% SOC and 100% SOC, respectively. A CNN model is developed based on impedance measured at 100% SOC [19]. All these models rely on impedances measured at specific SOC, making them dependent on accurate SOC determination.

Prior research has investigated how SOC influences EIS, presenting various polynomial regression models of different order for ohmic resistance, interface resistance, charge transfer resistance, and diffusion resistance [20]. For nickel–cobalt–aluminum (NCA) batteries, ohmic and interface resistances appear to be minimally impacted by SOC, while charge transfer resistance and diffusion resistance demonstrate notable SOC dependence [21]. Similar results in LiFePO₄ (LFP) batteries indicate that the first semicircle in the impedance shows no significant SOC dependency, but the second semi-circle is notably affected by SOC [22], [23]. This SOC influence on EIS impedance commonly used for battery capacity estimation highlights the necessity of incorporating SOC in the battery capacity estimation process. Conventional approaches exploiting features from middle and low-frequency impedance have considerable inaccuracies in battery capacity estimation when the BMS’s SOC estimation flaws.

The precision of SOC estimation was notably enhanced through the recent adoption of advanced adaptive filter methods

[24], with SOC errors remaining below 3% in various application scenarios. Nevertheless, specific circumstances can still result in considerable SOC inaccuracies. Hardware malfunctions in the electrically erasable programmable read-only memory (EEPROM) may prevent the preservation of SOC values. Upon BMS reactivation, an incorrect SOC value is utilized, leading to significant SOC errors. Substantial SOC discrepancies also occur when the BMS experiences an unexpected power supply disconnection, preventing the completion of the standard power-off procedure and the saving of SOC to the EEPROM [25]. The third scenario pertains to long-term, low-current battery discharge, where errors in the current sensing circuit can yield substantial SOC discrepancies [26]. Given the potential significant impact of these SOC errors, it is imperative to develop battery capacity estimation models that are insensitive to SOC estimation errors.

To mitigate the influence of SOC errors on battery capacity estimation accuracy, we first select impedance features that have a high correlation with battery aging and are insensitive to the partial SOC range, as determined by feature consistency analysis across different SOC, which concluded that there is minimal difference in impedance within the 20% to 50% SOC range. This leads to the development of the partial-range SOC-insensitive model using a transformer neural network. However, this model cannot handle scenarios where significant SOC errors occur; in such cases, the impedance measured under large SOC errors cannot be used as inputs for the partial-range SOC-insensitive model. To address this limitation, we develop a model that can recognize whether changes in EIS are caused by large SOC errors, leading to the development of the EIS change pattern model using k-nearest neighbors (KNN). This model can filter out impedance changes caused by incorrect SOC, ensuring that the partial-range SOC-insensitive model remains unaffected by large SOC errors. The implementation process of the proposed models is illustrated in Fig. 1. In this figure, Z_{t-1} and Z_t represent the partial-range SOC-insensitive features from the previous measurement Z_{t-1} and the current cycle’s measurement, respectively. The interval between the two measurements spans 50 cycles, as battery aging is a gradual process. After 50 cycles from the Z_{t-1} measurement, the process of

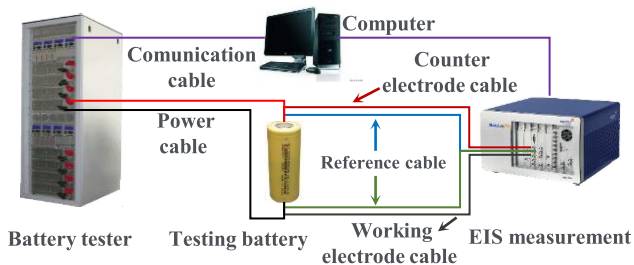


Fig. 2. Experimental setup.

obtaining Z_t and estimating capacity is carried out. To the best of our knowledge, this is the first study to realize EIS-based battery capacity estimation considering the multi-SOC analysis. The article makes the following contributions:

- 1) Introduction of a partial-range SOC-insensitive model, realized through the transformer model and incorporating a novel projector layer, enables accurate battery capacity estimation within the 20% to 50% SOC range.
- 2) Proposal of an EIS change pattern recognition model, realized through the KNN model, capable of identifying EIS alterations stemming from aging-based, SOC-based, and SOC-aging-based patterns.
- 3) Introduction of a feature extraction methodology that can extract features strongly correlated with battery aging, maintains consistent performance across diverse battery cells, and remains insensitive to partial SOC ranges.

The article is structured as follows: Section II presents the battery dataset, while Section III elaborates on the feature extraction process. Methodologies for capacity estimation and EIS change pattern recognition are detailed in Section IV. Section V presents the outcomes of capacity estimation, and finally, the article concludes in Section VI.

II. BATTERY DATASETS

The dataset utilized in this study includes EIS and battery capacity data obtained from four independent institutions, as referenced [27]. All four institutions use the same battery, EIS testing procedure, and a similar experimental setup to generate the dataset, as illustrated in Fig. 2. The battery studied is the $\text{LiNi}_{0.8}\text{Co}_{0.1}\text{Mn}_{0.1}$ (NMC 811) cell with a 18650 format and a nominal capacity of 3000 mAh. EIS measurements are conducted at six SOC levels: 20%, 35%, 50%, 65%, 80%, and 100%. The tests are performed at a temperature of 23 °C, with a frequency range extending from 0.02 to 20 kHz, covering 61 different frequency points. To ensure the reliability of the EIS data, a relaxation time of 30 min is maintained before each measurement. Different aging conditions of battery cells are used, such as aging temperature and depth of discharge (DoD), as detailed in Table I. Additionally, the label of batteries and the measurement equipment used by the four institutions are different, see the details in Table II. Eight cells from Institution 1, labeled as C05, C06, C09, C10, C11, C13, C17, and C19, are used for training and testing the models. Six cells from the other three institutions, labeled as C07, C12, C01, C02, C03, and C04, are used to verify the generality of the proposed models.

TABLE I
BATTERY AGING CONDITIONS (FROM [27])

Aging Condition	Cycle Temperature	DoD	Discharge and Charge Current	Battery Label
Condition 1	45°C	0%-100%	4 A	C01-C07
Condition 2	35°C	0%-100%	4 A	C09-C11
Condition 3	45°C	25%-75%	4 A	C13, C17, C19
Condition 4	45°C	30%-100%	4 A	C12

TABLE II
DIFFERENCES IN DATASET FROM FOUR INSTITUTIONS

Item	Name of Institutions			
	PTB	CMI	LNE	METAS
Location	Germany	Czech	France	Switzerland
Cycling equipment	Modulab MACCOR	BaSyTec XCTS	BioLogic MPG-205	MACCOR
EIS equipment	Modulab MACCOR	Zahner Zennium	BioLogic SP-200	BioLogic MPG-205
Battery Label	C05, C06, C09- C13, C17, C19	C07 C12	C01 C02	C03 C04
Purpose	Train and test models	Verify the generality of the models		

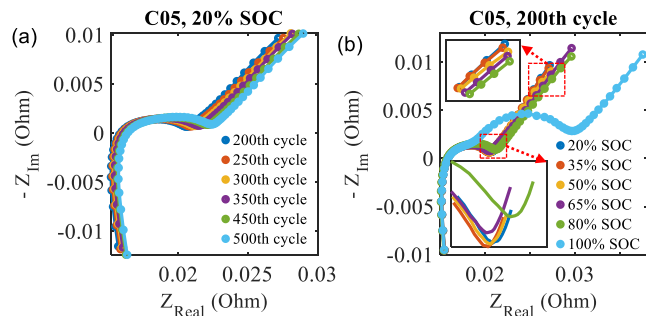


Fig. 3. EIS changes of cell C05 due to: (a) Battery aging; (b) SOC variations.

Fig. 3(a) and 3(b) portrays the EIS curves of battery cell C05 showing the impedance changes due to both battery aging and SOC variations. The figures demonstrate that EIS curves are influenced by both battery aging and SOC. With battery aging, the impedance at all frequencies escalates. As SOC increases, particularly within the middle and high SOC range, the middle and low-frequency components of impedance also increase. However, there is minimal disparity in impedance across different SOC levels in the high-frequency segment.

III. EXTRACTING FEATURES FROM EIS DATA

The primary aim of feature extraction is to pinpoint the critical frequency components of EIS impedance that contain the best information regarding battery aging. According to Fig. 4, three steps are involved in extracting useful features. First, correlation analysis is conducted to identify features strongly correlated with battery aging. Next, feature consistency analysis is performed across different battery cells to ensure that the extracted feature values maintain high consistency at the same

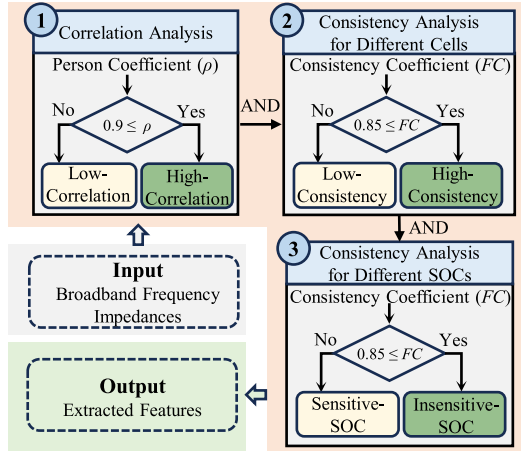


Fig. 4. Feature extraction methodology consists of three steps: first, correlation analysis; second, assessing feature consistency across different cells; and third, evaluating feature consistency across different SOC levels.

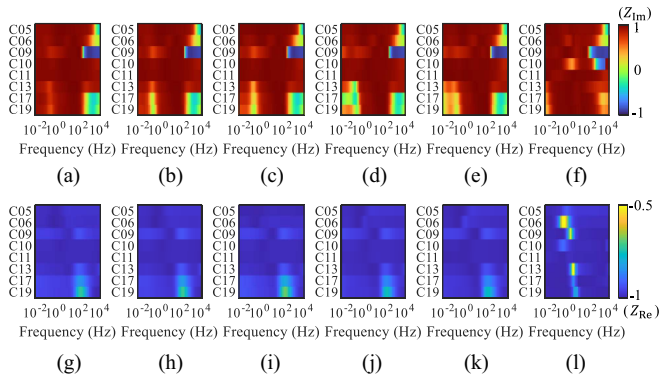


Fig. 5. Correlation analysis (ρ) results of broadband frequency impedance measured at different SOC levels for eight cells. (a)–(f) Correlation analysis results of imaginary part impedance (Z_{Im}). (g)–(l) Correlation analysis results of real part impedance (Z_{Re}). Analyses are conducted at 20% SOC, 35% SOC, 50% SOC, 65% SOC, 80% SOC, and 100% SOC, respectively.

battery capacity for various battery cells. Finally, a feature consistency analysis is carried out across different SOC levels to assess their sensitivity to SOC. High feature consistency across different SOC levels implies minimal impedance variation, qualifying such features as SOC-insensitive over the range in SOC considered.

A. Feature Correlation Analysis

The Pearson correlation coefficient (ρ) is utilized to assess the correlation between impedance at different frequencies and battery capacity. For feature extraction across various SOC levels, a correlation analysis is conducted on broadband frequency impedance at specific SOC levels—20%, 35%, 50%, 65%, 80%, and 100%. Moreover, correlation analysis encompasses both the imaginary and real parts of the impedance.

Fig. 5(a) shows that the EIS measurement at 20% SOC reveals a strong positive correlation between the low and

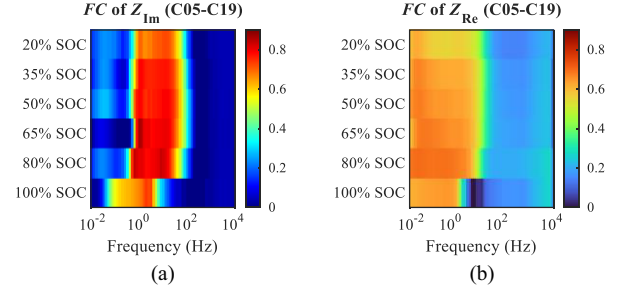


Fig. 6. Feature consistency (FC) analysis of broadband frequency impedance for all cells as a function of SOC level. (a) Z_{Im} . (b) Z_{Re} .

middle-frequency portions of the imaginary impedance and battery capacity across all eight battery cells. As the SOC increases, as illustrated in Fig. 5(b)–5(f), it is evident that only the middle-frequency section of the imaginary impedance maintains a robust correlation with battery capacity. Conversely, Fig. 5(g)–5(l) depict a significant negative correlation between the battery capacity and the low-, middle-, and very high-frequency segments of real impedance across the eight battery cells.

B. Feature Consistency Analysis for Different Battery Cells

Feature consistency analysis is another important indicator to assess feature quality [15]. A large value of the feature consistency coefficient (FC) indicates good similarity of feature values at the same battery capacity for different battery cells. For the given k_{th} feature, the FC is given by

$$FC_k = \frac{\sum_{j=1}^{N-1} \sum_{i=1}^{N-j} \frac{2\sigma_{f_{k_i}, f_{k_{i+j}}}}{(\bar{f}_{k_i} - \bar{f}_{k_{i+j}})^2 + \sigma_{f_{k_i}}^2 + \sigma_{f_{k_{i+j}}}^2}}{C_N^2} \quad (1)$$

where N is the total number of cells, i the i th cell, C_N^2 the total number of N batteries arranged in pairs, f_k the k th cell feature, f_{k_i} the k th feature of the i th cell with \bar{f}_{k_i} its average value, $\sigma_{f_{k_i}}^2$ the standard deviation of f_{k_i} , and $\sigma_{f_{k_i}, f_{k_{i+j}}}^2$ the covariance of f_{k_i} and $f_{k_{i+j}}$.

Referring to Fig. 6(a) and 6(b), it is evident that the middle-frequency imaginary impedance exhibits higher feature consistency at different SOC levels for the eight battery cells compared with the real impedance. Thus, only the imaginary impedance will be considered as feature candidates. The high-frequency impedance primarily reflects the characteristics of cell components, including electrolytes, current collectors, separators, and active material. This serves as the main distinguishing factor between different cells [5], [20]. On the other hand, the middle-frequency impedance is influenced by solid-electrolyte-interphase (SEI) layers and charge transfer process, which are relatively similar across all cells due to the comparable behavior of the active material [28]. Consequently, the results of our consistency analysis can be explained by the underlying electrochemistry mechanisms.

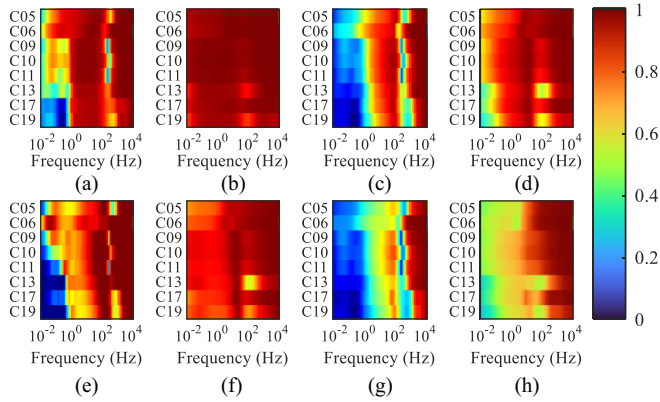


Fig. 7. Correlation analysis (FC) results of different features for eight cells. (a) and (b) FC of Z_{Im} and Z_{Re} among 20% to 50% SOC, respectively. (c) and (d) FC of Z_{Im} and Z_{Re} among 20% to 80% SOC, respectively. (e) and (f) FC of Z_{Im} and Z_{Re} among 65% to 80% SOC, respectively. (g) and (h) FC of Z_{Im} and Z_{Re} among 20% to 100% SOC, respectively.

TABLE III

RESULTS OF FEATURES EXTRACTION ANALYSIS FROM THE EIS DATA FOR BATTERY CAPACITY ESTIMATION

Diff-erent SOC's	Imaginary Part of Impedance (Ohm)			Result
	Correlation Analysis	Consistency Analysis (for Differ. Cells)	Consistency Analysis (for Differ. SOC's)	
20%	$Z(4-126 \text{ Hz})$	$Z(5-20 \text{ Hz})$	$Z(5-20 \text{ Hz})$	$Z(5-20 \text{ Hz})$
35%	$Z(5-159 \text{ Hz})$	$Z(1-32 \text{ Hz})$	$Z(5-20 \text{ Hz})$	$Z(5-20 \text{ Hz})$
50%	$Z(5-126 \text{ Hz})$	$Z(0.8-32 \text{ Hz})$		$Z(5-20 \text{ Hz})$
65%	$Z(5-159 \text{ Hz})$	$Z(0.8-32 \text{ Hz})$		$Z(5-20 \text{ Hz})$
80%	$Z(4-159 \text{ Hz})$	$Z(0.8-20 \text{ Hz})$	$Z(5-20 \text{ Hz})$	$Z(5-20 \text{ Hz})$
100%	$Z(0.1-0.4 \text{ Hz})$ $Z(40-80 \text{ Hz})$	$Z(1.6-3.2 \text{ Hz})$	$Z(3981-10000 \text{ Hz})$	/

C. Feature Consistency Analysis for Different SOC's

To identify the frequency of impedance that is insensitive to SOC, feature consistency analysis for different SOC's is conducted, considering four SOC clusters: feature consistency among 20%, 35%, and 50% SOC; among 20% to 80% SOC; among 20% to 100% SOC; and among 65% to 80% SOC. Analysis results, as depicted in Fig. 7(a) and 7(b), reveal that both middle and high-frequency parts of imaginary and real impedance exhibit high consistency among 20%, 35%, and 50% SOC, designating them as SOC-insensitive features within this range. However, with increasing SOC, Fig. 7(c) and 7(d) indicate decreasing consistency in the middle-frequency parts from 0.9 to 0.8. Meanwhile, Fig. 7(g) and 7(h) show that only high-frequency parts maintain consistent behavior from 20% SOC to 100% SOC.

D. Feature Extraction Results for Battery Capacity Estimation

Table III shows the features extracted through correlation analysis, consistency analysis for different battery cells, and consistency analysis for different SOC's, with e.g. $Z(5-20 \text{ Hz})$ the imaginary impedance in the extracted features ranging from

5 to 20 Hz. Thus, the middle-frequency parts of impedance from the imaginary are most promising: high correlation with battery capacity, consistency across different cells, and insensitivity to SOC within a specified range. $Z(5-20 \text{ Hz})$ is thus considered extracted features for the transformer neural network model of battery capacity estimation.

E. Feature Analysis for EIS Change Pattern Recognition

To distinguish between EIS changes caused by battery aging and those caused by SOC changes, it is essential to identify specific frequency parts of impedance as features to reflect these two patterns. As shown in Fig. 3, it is evident that all frequency parts of impedance are influenced by battery aging, whereas only the middle and low-frequency parts of impedance are affected by SOC. The different frequency ranges reflect the electrochemical mechanisms behind the influence of SOC on the EIS curve.

- 1) *High-Frequency Parts*: represent the sum of the ohmic resistance of the current collector, active material, and electrolyte. The influence of SOC on the ohmic resistance of the battery is small [20].
- 2) *First Semicircle Part*: relates to the SEI layer, the interface resistance varies slightly with SOC. This is because the composition and performance of the SEI membrane are highly dependent on the electrolyte composition. For a fresh cell at a constant temperature, the SEI remains relatively stable during the discharge process [20].
- 3) *Second Semicircle Part*: relates to the charge transfer process, with the relationship between charge transfer resistance (R_{ct}) and potential given by [29]

$$R_{ct} = \frac{1}{f F k_o A C_O^{0.5} C_R^{0.5}} \quad (2)$$

$$C_T = C_O + C_R \quad (3)$$

where C_O is the unoccupied intercalation sites, C_R is the concentration of Li ions, C_T is the total concentration of available intercalation sites. When C_O approaches C_T , or when C_R approaches C_T , this results in a rapid change of R_{ct} . Hence, the second semi-circle part of impedance is sensitive to SOC [30].

- 4) *Low-Frequency Parts*: relate to the diffusion resistance. At high SOC, the diffusion resistance increases significantly, likely because the concentration gradient of reactants diminishes as the battery approaches the end of charging. According to Fick's first law, a decrease in concentration gradient leads to a reduction in diffusion velocity, which is observed as an increase in diffusion resistance [20].

Based on this analysis, both the high and very low-frequency parts of impedance, specifically from the real parts, are selected as features for developing the EIS change pattern recognition model. The low-frequency range of features spans from 0.020 to 0.040 Hz, while the high-frequency range is from 1995 to 3981 Hz. Since the above electrochemical mechanisms are universal across different battery materials and are not related to battery

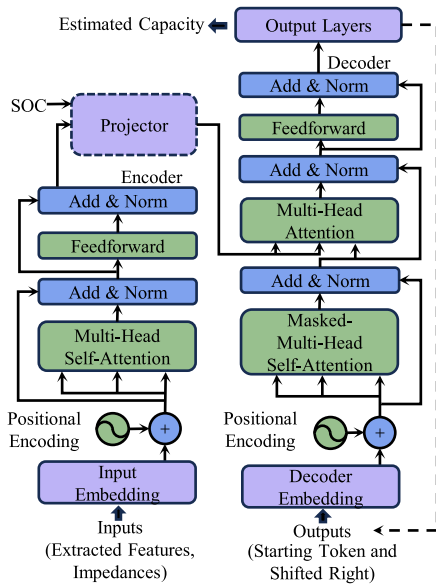


Fig. 8. Transformer neural network architecture for capacity estimation.

capacity, the extracted features have the potential to be used for batteries with various capacities and material systems.

IV. PROPOSED METHODOLOGY

The features extracted are utilized as inputs for data-driven methods aimed at achieving battery capacity estimation and EIS change pattern recognition. Typically, regression algorithms are employed for estimation tasks, whereas classification algorithms are utilized for pattern recognition tasks. In this study, we employ the transformer neural network and the KNN algorithm to accomplish these objectives.

A. Transformer Neural Network

The transformer neural network, widely used in natural language processing and computer vision, tackles the long-term dependency problem and additionally enhances training speed through parallel processing, unlike conventional methods such as LSTM, owing to its multihead attention architecture [31]. As a result, the transformer neural network can be utilized for battery capacity estimation, as illustrated in Fig. 8.

The detailed transformer neural network implementation process consists of six main steps. First, the input embedding layer incorporates the extracted features as input. Second, the positional encoding layer introduces positional encoding into the output. Third, the encoder layer is realized through the multihead self-attention layer and the feed-forward layer. Fourth, in comparison with traditional architectures, a novel projector layer has been added, which integrates SOC information as input to the decoder layer. Additionally, the decoder layer encompasses the masked multihead self-attention layer and cross-attention layer. Finally, the ultimate output layer is capable of furnishing the estimated battery capacity.

B. k -Nearest Neighbors

KNN is a supervised learning algorithm employed for classification. It determines the correct class for the test data by computing the distance between the test data and all training points [32]. The detailed implementation is as follows.

- 1) Set the parameter k , representing the number of neighbors. In this article, k is set to 3 to balance the model's bias and variance.
- 2) Calculate the Euclidean distance between the test data point and each training point.
- 3) Select the k neighbors to the test data point.
- 4) Predict the category of the test data point based on the majority category of the neighbors.

V. RESULTS AND DISCUSSIONS

The estimation accuracy is quantified using root-mean-square percentage error (RMSPE), maximum absolute error (MAXE), and maximum absolute percentage error (MAXPE) for each method.

A. Effectiveness of Extracted Features

The single SOC-based model is employed to assess the effectiveness of the extracted features. This model is constructed based on features measured at a specific SOC point, such as the 20% SOC-based model. In this model, the training input comprises the extracted features $Z(5-20\text{ Hz})$ measured at the 20% SOC. Notably, the projector element of the Transformer neural network architecture is not utilized for the single SOC-based model, resulting in input features without SOC labels.

A total of five single SOC-based models are developed, namely the 20% SOC-based model, 35% SOC-based model, 50% SOC-based model, 65% SOC-based model, and 80% SOC-based model. Due to significant differences in impedance between 100% SOC and other SOC levels, the 100% SOC-based model is not studied. These models are constructed using extracted features $Z(5-20\text{ Hz})$ measured at the respective SOC points: 20%, 35%, 50%, 65%, and 80%. The training is conducted using data from four battery cells (C05, C06, C09, and C10), and testing is performed on four other battery cells (C11, C13, C17, and C19). To examine the influence of SOC on these models, testing inputs include features measured at various SOCs. For instance, a 20% SOC-based model is tested with features from 20%, 35%, 50%, 65%, 80%, and 100% SOC. Similar testing conditions are applied to the other models, with results presented in Table IV.

For the 20% SOC-based model, when the input features are measured at 20% SOC, the maximum RMSPE among C11, C13, C17, and C19 is 2.17%. This indicates that the 20% SOC-based model accurately estimates battery capacity when the SOC of the testing battery cells is also 20%. Furthermore, when the input features are measured at 35% SOC and 50% SOC, the maximum RMSPE among the four testing battery cells is 2.18%. These findings demonstrate that the 20% SOC-based model achieves accurate battery capacity estimation even when the SOC of the testing battery cells differs from that of the

TABLE IV
CAPACITY ESTIMATION RMSPE FOR DIFFERENT SINGLE SOC-BASED TRANSFORMER MODELS

Inputs		Single SOC-based Transformer Model				
Features at diff. SOCs (Ohm)	Test Cells	20%	35%	50%	65%	80%
		SOC-Based Model	SOC-Based Model	SOC-Based Model	SOC-Based Model	SOC-Based Model
$Z(5-20\text{ Hz})$ (20% SOC)	C11	2.17%	3.49%	2.81%	4.59%	5.39%
	C13	1.60%	1.55%	1.80%	1.93%	3.37%
	C17	1.58%	2.07%	2.15%	2.31%	0.67%
	C19	1.02%	0.46%	0.41%	0.56%	2.12%
$Z(5-20\text{ Hz})$ (35% SOC)	C11	2.11%	2.44%	2.52%	5.17%	5.17%
	C13	1.14%	1.06%	1.36%	1.52%	3.15%
	C17	1.08%	1.56%	1.68%	1.86%	0.41%
	C19	1.51%	0.92%	0.73%	0.33%	2.39%
$Z(5-20\text{ Hz})$ (50% SOC)	C11	2.18%	1.87%	1.96%	4.39%	4.36%
	C13	0.46%	0.57%	0.97%	1.18%	2.73%
	C17	1.65%	2.01%	1.97%	2.06%	0.26%
	C19	0.74%	0.28%	0.15%	0.39%	1.86%
$Z(5-20\text{ Hz})$ (65% SOC)	C11	2.99%	3.09%	2.75%	3.44%	3.63%
	C13	0.28%	0.50%	0.71%	1.00%	2.46%
	C17	1.82%	2.25%	2.06%	1.67%	0.40%
	C19	1.14%	0.66%	0.61%	0.53%	1.64%
$Z(5-20\text{ Hz})$ (80% SOC)	C11	5.28%	5.00%	4.78%	3.19%	2.15%
	C13	2.26%	2.11%	1.53%	1.51%	1.32%
	C17	3.46%	3.68%	3.33%	3.38%	1.46%
	C19	1.68%	2.01%	1.62%	1.85%	0.34%
$Z(5-20\text{ Hz})$ (100% SOC)	C11	11.27%	14.00%	15.30%	8.89%	9.15%
	C13	11.67%	13.27%	17.34%	8.16%	7.24%
	C17	12.93%	12.48%	14.60%	9.13%	7.99%
	C19	12.62%	11.92%	14.07%	8.80%	7.72%

training battery cells. Similar results are observed for the 35% SOC-based model and the 50% SOC-based model. Therefore, the extracted features $Z(5-20\text{ Hz})$ exhibit SOC insensitivity within the SOC range from 20% to 50%.

Fig. 9(a) illustrates the performance of a 50% SOC-based model when input features are measured at 20% SOC, 35% SOC, and 50% SOC, all the battery cells can achieve accurate battery capacity estimation. However, for the 20% SOC-based model, the 35% SOC-based model, and the 50% SOC-based model, when input features are measured at 65% SOC, 80% SOC, and 100% SOC, the maximum RMSPEs are 3.09%, 5.28%, and 15.30%, respectively. Thus, significant differences in SOC between the input features of testing battery cells and training battery cells result in substantial battery capacity errors, especially when the SOC of the testing battery cells is 100% (which supports our choice of not studying the 100% SOC-based model). These results are depicted in Fig. 10(a) and 10(b).

For the 65% SOC-based model and the 80% SOC-based model, when input features are measured at 65% SOC and 80% SOC, the maximum RMSPE is 3.63%. These results indicate that both models can accurately estimate battery capacity when the input features are measured within the range of 65% SOC to 80% SOC. However, when input features are measured at 20% SOC, 35% SOC, 50% SOC, and 100% SOC, the maximum RMSPE for the four battery cells is 5.39%, 5.17%, 4.39%, and 9.15%, respectively. Consequently, when the input features are measured at low and high SOCs, a larger SOC error occurs [Fig. 10(c) and 10(d)].

Next to the impact of different SOC ranges on the proposed models, the influence of various aging conditions on the proposed models is also discussed. The above capacity estimation results indicate that even though the testing battery cells experience different aging conditions from the training cells, the models still demonstrate accurate estimation capabilities. This suggests that aging factors, such as temperature and DoD, do not significantly impact the relationship between battery impedance and aging status. Additionally, as highlighted [16], the aging current profile does not substantially impact this relationship. Consequently, the proposed models can be applied to battery cells subjected to various aging conditions, as long as their EIS measurement conditions are consistent.

In summary, the effectiveness of using $Z(5-20\text{ Hz})$ for capacity estimation in batteries under various aging conditions is evident. Notably, it accurately estimates battery capacity even when the SOC of the testing battery cells differs from that of the training battery cells, especially within the SOC range of 20% to 50%.

B. Effectiveness of Partial-Range SOC-Insensitive Model

In the training of a single SOC-based transformer model, the input features are measured at a specific SOC point. However, it is expected that a hybrid SOC-based transformer model, trained by input features from various SOC points, will perform even better. Consequently, the projector element of the transformer neural network architecture is required, resulting in input features with SOC labels.

The hybrid SOC-based model is trained using data from four battery cells: C05, C06, C09, and C10. The input variables for training include extracted features and SOC labels, considering three SOC levels—20%, 35%, and 50%. Subsequently, the model is tested on four battery cells: C11, C13, C17, and C19. The input variables for testing battery cells also include extracted features and SOC. Table V outlines different testing cases. In the first testing case, the input features are measured at 20% SOC, denoted as $Z(5-20\text{ Hz})$ (20% SOC), while the SOC label encompasses all three levels (20%, 35%, and 50%). This case aims to evaluate the model's accuracy in estimating battery capacity when the SOC label does not precisely match the input features. The second and third testing cases involve input features measured at 35% SOC and 50% SOC, respectively, with SOC labels covering the three levels.

The hybrid SOC-based model consistently achieves accurate battery capacity estimation across all testing cases. When the input features match the SOC label, the maximum RMSPE is 2.29%, while mismatched input features and SOC labels result in a maximum RMSPE of 2.69%. Fig. 9(b) displays the capacity estimation results for the second testing case. In summary, the hybrid SOC-based model demonstrates robust capacity estimation and insensitivity to partial SOC variations.

C. Evaluation of the EIS Change Pattern Recognition Model

To train the model capable of recognizing the three patterns of EIS change, namely, aging-based, SOC-based, and

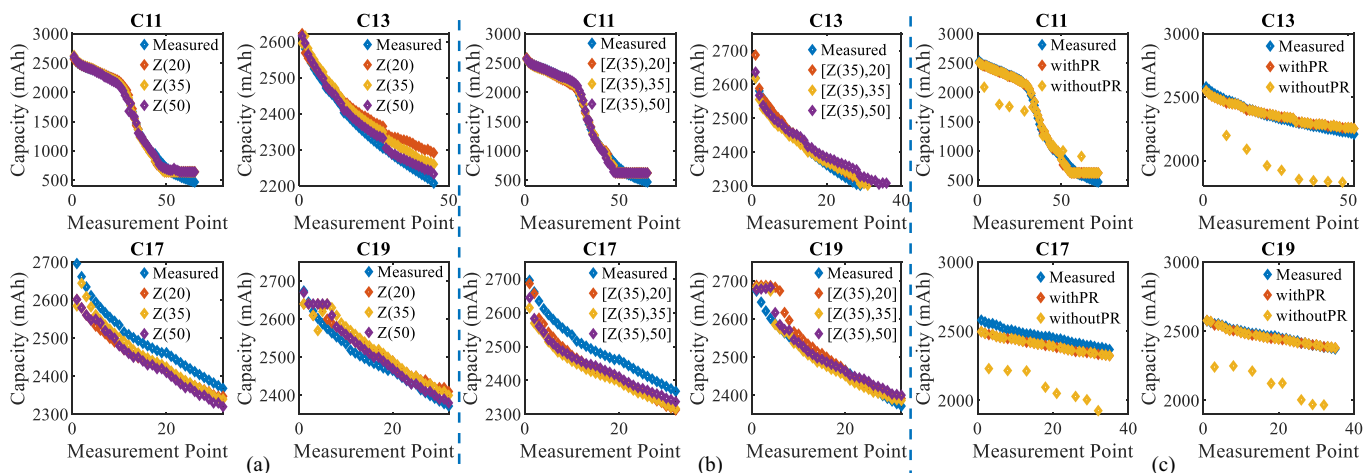


Fig. 9. Battery capacity estimation results of C11, C13, C17, and C19. (a) Results of 50% SOC-based model when input features are measured at 20%, 35%, and 50% SOC. (b) Results of hybrid SOC-based model, the input features are measured at 35% SOC, denoted as Z (35% SOC), while the SOC label includes all three levels (20%, 35%, and 50%). (c) Battery capacity estimation results are based on two methods: the first uses only the partial-range SOC-insensitive model without a pattern recognition (PR) model, while the second includes the PR model.

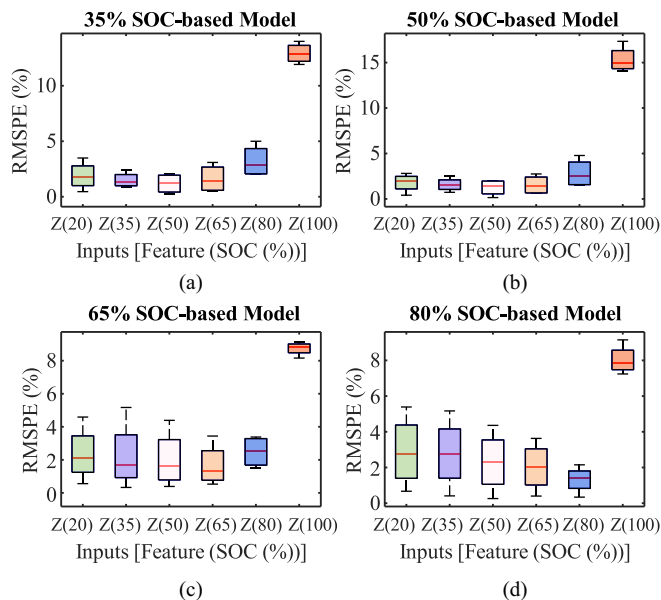


Fig. 10. RMSPE distributions of the battery capacity estimation (cell C11, C13, C17, and C19) for different single SOC-based transformer models using Z (5-20 Hz). Specifically, Z (20), Z (35), Z (50), Z (65), Z (80), and Z (100) denote the impedance features measured at 20% SOC, 35% SOC, 50% SOC, 65% SOC, 80% SOC, and 100% SOC, respectively.

SOC-aging-based, the training datasets must be prepared. For the Aging-based category, the training dataset is generated based on the delta impedance between two impedance measurement points taken at 50% SOC and a measurement interval of 50 cycles. Similarly, for the SOC-based category, the training dataset is created based on the delta impedance between the impedance measured at 100% SOC and the impedance measured at 50% SOC, where the impedance of two different SOC is measured at the same battery aging level. The training dataset for the SOC-Aging-based category is again based on the delta impedance between the impedance measured at 100% SOC and the impedance measured at 50% SOC, but now at different

TABLE V
CAPACITY ESTIMATION RMSPE FOR HYBRID SOC-BASED TRANSFORMER MODEL

Test Conditions		Test Cells			
Features (Ohm)	SOC Label	C11	C13	C17	C19
Z (5-20 Hz) (20% SOC)	20%	2.00%	0.95%	2.29%	0.74%
	35%	2.14%	1.23%	2.69%	0.61%
	50%	2.52%	1.65%	2.24%	0.50%
Z (5-20 Hz) (35% SOC)	20%	1.83%	0.41%	1.80%	1.23%
	35%	1.91%	0.70%	2.25%	0.67%
	50%	2.27%	1.16%	1.78%	0.75%
Z (5-20 Hz) (50% SOC)	20%	2.23%	0.50%	2.41%	0.72%
	35%	2.02%	0.66%	2.62%	0.71%
	50%	1.90%	0.73%	2.07%	0.31%

aging levels, 50 cycles apart. Four battery cells—C05, C06, C09, and C10—are utilized for creating the training dataset, while another four battery cells—C11, C13, C17, and C19—are employed for creating the testing dataset.

The extracted features for the EIS change pattern recognition model comprise real impedance values measured at both high and low frequencies, specifically ranging from 0.020 to 0.040 Hz and from 1995 to 3981 Hz. To visualize the distribution of the three patterns, a scatter diagram is presented based on one low-frequency impedance value and one high-frequency impedance value, as depicted in Fig. 11(a). It is evident that both the high and low-frequency impedance values increase with battery aging for the aging-based pattern. However, in the SOC-based pattern, the low-frequency impedance value exhibits a noticeable increase compared with the higher frequency. Consequently, the extracted features facilitate the recognition of the Aging-based and SOC-based patterns. While there are discernible differences between the SOC-based and SOC-aging-based patterns, some points pose a challenge for the features to entirely distinguish between the SOC-based and SOC-aging-based categories. Nevertheless, this challenge does not affect the distinction between SOC-based and aging-based patterns.

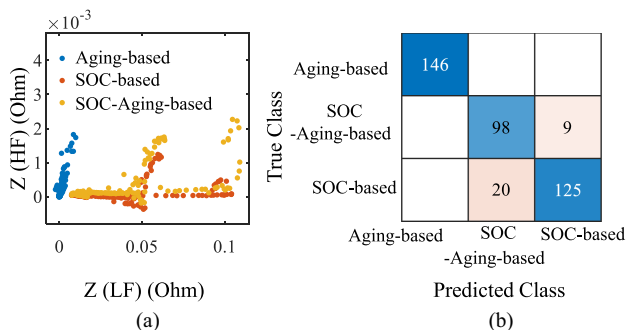


Fig. 11. (a) Scatter diagram of three EIS change patterns based on the low-frequency (LF) and high-frequency impedance (HF). (b) Results of EIS change pattern recognition model for cells C11, C13, C17, and C19.

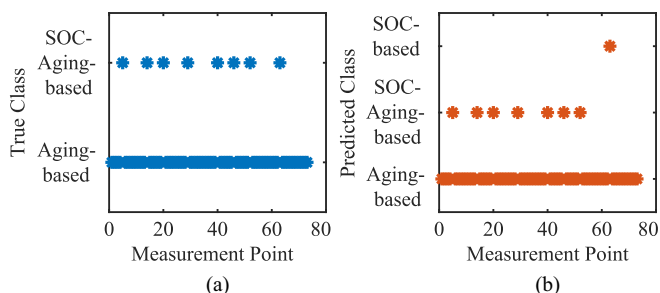


Fig. 12. Results of EIS change pattern recognition model for cell C11. Eight impedance points measured at 100% SOC are introduced into the impedances measured at 50% SOC. (a) True class. (b) Predicted class.

Fig. 11(b) presents the results of the EIS change pattern recognition model. The number in the figure represents the number of samples. The class accuracy for the Aging-based category is 100%. For the SOC-aging-based and SOC-based patterns, the class accuracy is 83.1% and 93.3%, respectively. Hence, the model effectively accomplishes EIS change pattern recognition.

D. Effectiveness of EIS Change Pattern Recognition Model in Capacity Estimation

The partial-range SOC-insensitive model demonstrates effectiveness within the SOC ranges of 20% to 50%. Furthermore, it maintains acceptable battery capacity estimation error within the SOC range of 65% to 80%. However, when the SOC reaches 100%, the partial-range SOC-insensitive model may yield a significant estimation error. Therefore, to mitigate this issue, the EIS change pattern recognition model should be employed. To evaluate the effectiveness of the EIS change pattern recognition model, eight impedance points measured at 100% SOC are introduced into the impedances measured at 50% SOC for the four testing battery cells (C11, C13, C17, and C19). Fig. 12 showcases the recognition results for cell C11, where the model successfully identifies the seven impedances belonging to the SOC-aging-based pattern. It is noteworthy that one impedance is classified as SOC-based, but this does not impact battery

TABLE VI
COMPARISON OF CAPACITY ESTIMATION ACCURACY OF TWO METHODS

Test Cells	Without Pattern Recognition Model		With Pattern Recognition Model	
	MAXE	MAXPE	MAXE	MAXPE
C11	565 mAh	18.9%	85.3 mAh	2.84%
C13	443 mAh	15.2%	44.1 mAh	1.47%
C17	456 mAh	15.2%	83.5 mAh	2.78%
C19	429 mAh	14.3%	16.6 mAh	0.55%

capacity estimation, as only impedances belonging to the aging-based pattern are utilized as input for the partial-range SOC-insensitive model.

Fig. 9(c) displays the results of battery capacity estimation for four battery cells using two methods. The first method solely relies on the partial-range SOC-insensitive model without integrating the EIS change pattern recognition model. Notably, the impedances measured at 100% SOC lead to a significant battery estimation error. Conversely, in the second method, the partial-range SOC-insensitive model is combined with the EIS change pattern recognition model, effectively mitigating the substantial battery estimation error caused by the impedances measured at 100% SOC.

Table VI presents the comparison results of the two methods, revealing that the maximum MAXE and MAXPE for the first method are 565 mAh and 18.9%, respectively, compared with respectively 85.3 mAh and 2.84% for the second method, indicating a reduction in MAXPE by 16%. This underscores the effectiveness of the proposed EIS change recognition model in enhancing battery capacity estimation.

E. Comparative Analysis With Different Methods Based on an Additional Dataset

To demonstrate the generality and superiority of the proposed methods, a comparative analysis with various existing methods is conducted using an additional dataset. The existing methods include the GPR-based model [10], the SVM-based model [11], the CNN-based model [12], and the LSTM-based model [13]. Both the proposed method and the existing models are trained on four battery cells: C05, C06, C09, and C10. The additional dataset, which includes cells C01-C04, C07, and C12, is used for testing. The first testing is conducted under the correct SOC scenario, where all impedances are measured at 50% SOC. Fig. 13(a) showcases the recognition results for cell C07, where the EIS change recognition model successfully identifies that all impedance changes belong to the Aging-based pattern. Table VII presents the battery capacity estimation accuracy using different methods. Fig. 13(b), derived from Table VII, shows that both the proposed methods and existing models can accurately estimate battery capacity under the correct SOC scenario.

The second testing is conducted under the incorrect SOC scenario, where eight impedance points measured at 100% SOC are introduced into the impedance measured at 50% SOC.

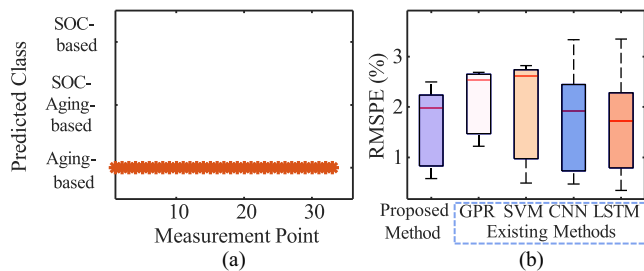


Fig. 13. Results of battery capacity estimation under the correct SOC scenario, where all impedance changes belong to the aging-based pattern. (a) Predicted class of EIS change pattern recognition model for C07. (b) RMSPE distributions of the battery capacity estimation (cells C01-C04, C07, C12) for the proposed method compared with different existing methods.

TABLE VII

CAPACITY ESTIMATION ACCURACY UNDER DIFFERENT METHODS

Methods	The Accuracy of Test Cells (RMSPE)					
	C01	C02	C03	C04	C07	C12
Proposed	2.24%	2.50%	0.58%	0.83%	2.20%	1.75%
GPR	2.65%	2.69%	1.47%	1.22%	2.55%	2.54%
SVM	2.82%	2.73%	0.49%	0.97%	2.74%	2.49%
CNN	1.90%	3.34%	0.47%	0.73%	2.45%	1.94%
LSTM	2.28%	3.35%	0.34%	0.79%	2.23%	1.23%

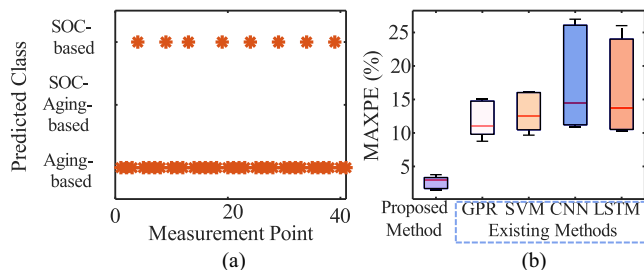


Fig. 14. Results of battery capacity estimation under an incorrect SOC scenario, where the changes in eight impedances belong to the SOC-based pattern. (a) Predicted class of EIS change pattern recognition model for C07. (b) MAXPE distributions of the battery capacity estimation (cells C01-C04, C07, C12) for the proposed method compared with different existing methods.

In this scenario, the impedance of two different SOC is measured at the same battery aging level. Fig. 14(a) showcases the recognition results for cell C07, where the model successfully identifies that the changes in the eight impedance points belong to the SOC-based pattern. Using a similar approach as in Fig. 13(b), we derive Fig. 14(b). Unlike Fig. 13(b), Fig. 14(b) uses MAXPE as the statistical indicator. As the eight SOC-based impedance points can cause outliers in incorrect SOC scenarios. Making MAXPE more appropriate than RMSPE. Fig. 14(b) demonstrates that our proposed method can still achieve accurate battery capacity estimation compared with existing methods, thanks to our EIS change pattern recognition model, which effectively removes the influence of impedance measured at incorrect SOC. In contrast, all existing methods show significant errors in battery capacity estimation, with a

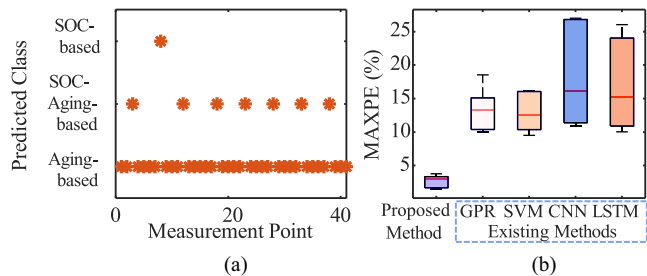


Fig. 15. Results of battery capacity estimation under the incorrect SOC scenario, where the changes in eight impedances belong to the SOC-aging-based pattern. (a) Predicted class of EIS change pattern recognition model for C07. (b) MAXPE distributions of the battery capacity estimation (cells C01-C04, C07, C12) for the proposed method compared with existing methods.

maximum error exceeding 10%, caused by the eight impedance points measured at 100% SOC.

The third testing is also conducted under the incorrect SOC scenario, where eight impedance points measured at 100% SOC are introduced into the impedance measured at 50% SOC. However, in this case, the impedance of the two different SOC is measured at different battery aging levels, 50 cycles apart. Fig. 15(a) showcases the recognition results for Cell C07, where the model successfully identifies that the changes in seven impedance points belong to the SOC-aging-based pattern, while one impedance point belongs to the SOC-based pattern. As previously discussed, only the aging-based pattern is used for battery capacity estimation, so these recognition results do not affect the accuracy of the battery capacity estimation. Once again, Fig. 15 demonstrates that our proposed method achieves a much better accurate battery capacity estimation than existing methods.

In summary, these results demonstrate the superiority of the proposed method compared with existing methods, particularly under incorrect SOC scenarios. Additionally, the results highlight the generality of the proposed method, showing its capability to handle additional datasets from different institutions and measured with different equipment.

VI. CONCLUSION

This article introduces partial-range SOC-insensitive models designed for accurate battery capacity estimation within the SOC range of 20% to 50%. Additionally, a novel EIS change pattern recognition model is proposed to identify EIS changes resulting from both battery aging and SOC variations. This recognition model serves as a complement to the partial-range SOC-insensitive model, aiding in the elimination of errors in battery capacity estimation, particularly when there are significant discrepancies in SOC between testing and training battery cells. To the best of our knowledge, this is the first study to present an EIS-based battery capacity model that overcomes errors due to SOC variations.

In our tests, the proposed hybrid SOC-based transformer neural network model achieves an RMSPE of less than 2.29% for all battery cells. Additionally, the EIS change pattern recognition model appears to successfully identify the Aging-based

pattern with 100% class accuracy. Due to the effectiveness of the EIS change pattern recognition model in battery capacity estimation, the MAXPE is less than 3% in cases with significant SOC errors, compared with a notable 19% when not utilizing the pattern recognition model. Finally, test results demonstrate the superiority of the proposed method compared with existing methods, especially under incorrect SOC scenarios.

REFERENCES

- [1] Q. Wang, Z. Wang, P. Liu, and L. Zhou, "A battery capacity estimation framework combining hybrid deep neural network and regional capacity calculation based on real-world operating data," *IEEE Trans. Ind. Electron.*, vol. 70, no. 8, pp. 8499–8508, Aug. 2023.
- [2] Y. Xie et al., "Coestimation of SOC and three-dimensional sot for lithium-ion batteries based on distributed spatial-temporal online correction," *IEEE Trans. Ind. Electron.*, vol. 70, no. 6, pp. 5937–5948, Jun. 2023.
- [3] Y. Li, Z. Wei, C. Xie, and D. M. Vilathgamuwa, "Physics-based model predictive control for power capability estimation of lithium-ion batteries," *IEEE Trans. Ind. Inform.*, vol. 19, no. 11, pp. 10763–10774, Nov. 2023.
- [4] Y. Che, F. Forest, Y. Zheng, L. Xu, and R. Teodorescu, "Health prediction for lithium-ion batteries under unseen working conditions," *IEEE Trans. Ind. Electron.*, vol. 71, no. 11, pp. 14254–14264, Nov. 2024.
- [5] P. Iurilli, C. Brivio, and V. Wood, "On the use of electrochemical impedance spectroscopy to characterize and model the aging phenomena of lithium-ion batteries: a critical review," *J. Power Sources*, vol. 505, 2021, Art. no. 229860.
- [6] J. A. A. Qahouq and Z. Xia, "Single-perturbation-cycle online battery impedance spectrum measurement method with closed-loop control of power converter," *IEEE Trans. Ind. Electron.*, vol. 64, no. 9, pp. 7019–7029, Sep. 2017.
- [7] D. A. Howey, P. D. Mitcheson, V. Yufit, G. J. Offer, and N. P. Brandon, "Online measurement of battery impedance using motor controller excitation," *IEEE Trans. Veh. Technol.*, vol. 63, no. 6, pp. 2557–2566, Jul. 2014.
- [8] M. Crescentini, A. De Angelis, R. Ramilli, A. Moschitta, and P. Carbone, "Online EIS and diagnostics on lithium-ion batteries by means of low-power integrated sensing and parametric modeling," *IEEE Trans. Instrum. Meas.*, vol. 70, pp. 1–11, 2021, Art. no. 2001711.
- [9] X. Tang et al., "Predicting battery impedance spectra from 10-second pulse tests under 10 Hz sampling rate," *IScience*, vol. 26, no. 6, 2023, Art. no. 106821.
- [10] Y. Zhang, Q. Tang, Y. Zhang, J. Wang, U. Stimming, and A. A. Lee, "Identifying degradation patterns of lithium ion batteries from impedance spectroscopy using machine learning," *Nat. Commun.*, vol. 11, no. 1, p. 1706, 2020.
- [11] C. Chang, S. Wang, J. Jiang, Y. Jiang, and L. Wang, "An improvement of equivalent circuit model for state of health estimation of lithium-ion batteries based on mid-frequency and low-frequency electrochemical impedance spectroscopy," *Measurement*, vol. 202, 2022, Art. no. 111795.
- [12] R. Xiong, J. Tian, W. Shen, J. Lu, and F. Sun, "Semi-supervised estimation of capacity degradation for lithium ion batteries with electrochemical impedance spectroscopy," *J. Energy Chemistry*, vol. 76, pp. 404–413, Jan. 2023.
- [13] W. Zhang, T. Li, W. Wu, N. Ouyang, and G. Huang, "Data-driven state of health estimation in retired battery based on low and medium-frequency electrochemical impedance spectroscopy," *Measurement*, vol. 211, 2023, Art. no. 112597.
- [14] Z. Ning, P. Venugopal, G. Rietveld, and T. B. Soeiro, "Transformer neural network for early battery capacity prediction based on electrochemical impedance spectroscopy," in *Proc. IEEE Int. Conf. Metrology eXtended Reality, Artif. Intell. Neural Eng. (MetroXRaine)*, Piscataway, NJ, USA: IEEE Press, 2023, pp. 329–334.
- [15] Z. Ning, P. Venugopal, G. Rietveld, and T. B. Soeiro, "Data-driven methods for robust battery capacity estimation based on electrochemical impedance spectroscopy," in *Proc. 25th Eur. Conf. Power Electron. (EPE ECCE Europe)*, Piscataway, NJ, USA: IEEE Press, 2023, pp. 1–8.
- [16] B. Jiang, J. Zhu, X. Wang, X. Wei, W. Shang, and H. Dai, "A comparative study of different features extracted from electrochemical impedance spectroscopy in state of health estimation for lithium-ion batteries," *Appl. Energy*, vol. 322, 2022, Art. no. 119502.
- [17] X. Su, B. Sun, J. Wang, W. Zhang, S. Ma, X. He, and H. Ruan, "Fast capacity estimation for lithium-ion battery based on online identification of low-frequency electrochemical impedance spectroscopy and Gaussian process regression," *Appl. Energy*, vol. 322, 2022, Art. no. 119516.
- [18] S. Kim, Y. Y. Choi, and J.-I. Choi, "Impedance-based capacity estimation for lithium-ion batteries using generative adversarial network," *Appl. Energy*, vol. 308, 2022, Art. no. 118317.
- [19] Z. Ning, P. Venugopal, T. B. Soeiro, and G. Rietveld, "Computation-light ai models for robust battery capacity estimation based on electrochemical impedance spectroscopy," *IEEE Trans. Transp. Electrific.*, vol. PP, no. 99, p. 1, Jan. 2024.
- [20] F. Feng, R. Yang, J. Meng, Y. Xie, Y. Chai, and L. Mou, "Electrochemical impedance characteristics at various conditions for commercial solid-liquid electrolyte lithium-ion batteries: Part 1. experiment investigation and regression Anal.," *Energy*, vol. 242, 2022, Art. no. 122880.
- [21] D. Andre, M. Meiler, K. Steiner, C. Wimmer, T. Soczka-Guth, and D. Sauer, "Characterization of high-power lithium-ion batteries by electrochemical impedance spectroscopy. i. Experimental investigation," *J. Power Sources*, vol. 196, no. 12, pp. 5334–5341, 2011.
- [22] X. Wang, X. Wei, and H. Dai, "Estimation of state of health of lithium-ion batteries based on charge transfer resistance considering different temperature and state of charge," *J. Energy Storage*, vol. 21, pp. 618–631, Feb. 2019.
- [23] Q.-K. Wang, Y.-J. He, X.-S. Hu, and Z.-F. Ma, "State of charge-dependent polynomial equivalent circuit modeling for electrochemical impedance spectroscopy of lithium-ion batteries," *IEEE Trans. Power Electron.*, vol. 33, no. 10, pp. 8449–8460, Oct. 2018.
- [24] Z. Ning, Z. Deng, and W. Guo, "Co-estimation of state of charge and state of health for 48 v battery system based on cubature Kalman filter and h-infinity," *J. Energy Storage*, vol. 56, 2022, Art. no. 106052.
- [25] B. Tarhan, O. Yetik, and T. H. Karakoc, "Hybrid battery management system design for electric aircraft," *Energy*, vol. 234, 2021, Art. no. 121227.
- [26] X. Lai, S. Wang, L. He, L. Zhou, and Y. Zheng, "A hybrid state-of-charge estimation method based on credible increment for electric vehicle applications with large sensor and model errors," *J. Energy Storage*, vol. 27, 2020, Art. no. 101106.
- [27] H. S. Chan, *Libforsecuse data release - impedance spectra of life cycle tests of commercial 18650 cells*, Zenodo, Accessed: Mar. 2022. [Online]. Available: <https://zenodo.org/records/6418665>
- [28] V. Muenzel et al., "A comparative testing study of commercial 18650-format lithium-ion battery cells," *J. Electrochem. Soc.*, vol. 162, no. 8, 2015, Art. no. A1592.
- [29] M. Levi, K. Gamolsky, D. Aurbach, U. Heider, and R. Oesten, "On electrochemical impedance measurements of LiCoO_2 , $\text{LiNi}_{0.8}\text{O}_2$ and $\text{LiNi}_{0.8}\text{O}_2$ intercalation electrodes," *Electrochimica Acta*, vol. 45, no. 11, pp. 1781–1789, 2000.
- [30] Q. Zhang, C.-G. Huang, and W. Peng, "Electrochemical impedance spectroscopy based state-of-health estimation for lithium-ion battery considering temperature and state-of-charge effect," *IEEE Trans. Transp. Electrific.*, vol. 8, no. 4, pp. 4633–4645, Dec. 2022.
- [31] A. Zeyer, R. Schlüter, and H. Ney, "A comparison of transformer and LSTM encoder decoder models for ASR," in *Proc. IEEE Autom. Speech Recognit. Workshop (ASRU)*, Piscataway, NJ, USA: IEEE Press, 2019, pp. 8–15.
- [32] Z. Zhang, "Introduction to machine learning: k-nearest neighbors," *Ann. Transl. Med.*, vol. 4, no. 11, p. 218, 2016.



Zhansheng Ning (Student Member, IEEE) received the bachelor's and master's degrees in mechatronic engineering from the University of Science and Technology, Beijing, China, in 2015 and 2018, respectively. He is currently working toward the Ph.D. degree in electrical engineering with Power Electronics and EMC Group, University of Twente, Enschede, The Netherlands.

From 2018 to 2022, he was a Battery Management Systems (BMS) Software Engineer with Gotion High-tech Company, Hefei, China.

From 2019 to 2020, he was also a Research Associate at Gotion-NTU Smart Energy Laboratory, Nanyang Technological University, Singapore. His research interests include the state estimation, modeling, and life prediction of Lithium-ion batteries.



Junyun Deng received the M.S. degree in microelectronics and solid-state electronics from the Chinese Academy of Sciences, Shanghai Institute of Microsystem and Information Technology, Shanghai, China, in 2020. He is currently working toward the Ph.D. degree in electrical engineering with Power Electronics and EMC Group, University of Twente, Enschede, The Netherlands.

His research interests include the applications of wide band gap semiconductors and high-power converter design using artificial intelligence methods.



Prasanth Venugopal (Senior Member, IEEE) received the Ph.D. degree in magnetic energy transfer inroads from Delft University of Technology, Delft, The Netherlands, in 2016.

From 2016 to 2018, he was a Senior Electrical Engineer in the field of power electronics with Qualcomm Halo, Munich, Germany. In 2019, he joined as a Technical Specialist for xEV applications with TDK Europe GmbH, Munich. Currently, he is an Assistant Professor with Power Electronics and EMC Group, University

of Twente, Enschede, The Netherlands. His research interests include battery electronics and EV charging systems.

Dr. Venugopal was an Associate Editor for IEEE TRANSACTIONS ON TRANSPORTATION ELECTRIFICATION.



Thiago Batista Soeiro (Senior Member, IEEE) received the Ph.D. degree in electrical engineering from Swiss Federal Institute of Technology, Zurich, Switzerland, in 2012.

From 2013 to 2018, he was a Senior Scientist with the Corporate Research Center, ABB Switzerland Ltd., Baden-Dattwil, Switzerland. From 2018 to 2022, he was an Associate Professor with DC Systems, Energy Conversion and Storage Group, Delft University of Technology, Delft, The Netherlands. Currently, he is a Full

Professor with Power Electronics and EMC Group, University of Twente, Enschede, The Netherlands. His research interests include advanced high-power converters and dc system integration.

Dr. Soeiro is a recipient of the 2013 IEEE Industrial Electronics Society Best Conference Paper Award, and the International Conference on Power Electronics and Motion Control 2020 and 2022 (PEMC 2020 and 2022).



Gert Rietveld (Senior Member, IEEE) received the Ph.D. degree in low temperature and solid-state physics from Delft University of Technology, Delft, The Netherlands, in 1993.

Since 1993, he has been with Van Swinden Laboratorium (VSL), National Measurement Institute of The Netherlands, Delft, where he is currently the Chief Scientist with Electricity and Time Department. He has more than 25 years of experience in the area of electrical metrology. Currently, he is also a Full Professor with

Power Electronics and EMC Group, University of Twente, Enschede, The Netherlands. His research interests include precision measurements on batteries and measurement of power converter efficiency.

Dr. Rietveld is an Active Member of Conseil International des Grands Réseaux Électriques (CIGRÉ), Comité Européen de Normalisation Électrotechnique (CENELEC), and International Electrotechnical Commission (IEC) working groups.